

# **1 A Non-homogeneous Time Mixed Integer LP**

## **2 Formulation for Traffic Signal Control**

3 Iain Guilliard  
4 National ICT Australia  
5 7 London Circuit  
6 Canberra, ACT, Australia  
7 iguilliard@nicta.com.au

8 Scott Sanner  
9 Oregon State University  
10 1148 Kelley Engineering Center  
11 Corvallis, OR 97331  
12 scott.sanner@oregonstate.edu

13 Felipe W. Trevizan  
14 National ICT Australia  
15 7 London Circuit  
16 Canberra, ACT, Australia  
17 felipe.trevizan@nicta.com.au

18 Brian C. Williams  
19 Massachusetts Institute of Technology  
20 77 Massachusetts Avenue  
21 Cambridge, MA 02139  
22 williams@csail.mit.edu

23 4516 words + 8 figures + 0 table + 24 citations  
24 (Weighted total words: 6516 out of 7000 + 35 references)  
25 August 1, 2015

## 1 **ABSTRACT**

2 As urban traffic congestion is on the increase worldwide, it is critical to maximize capacity and  
3 throughput of existing road infrastructure through optimized traffic signal control. To this end, we  
4 build on the body of work in mixed integer linear programming (MILP) approaches that attempt to  
5 jointly optimize traffic signal control over an entire traffic network and specifically on improving  
6 the scalability of these methods for large numbers of intersections. Our primary insight in this work  
7 stems from the fact that MILP-based approaches to traffic control used in a receding horizon control  
8 manner (that replan at fixed time intervals) need to compute high fidelity control policies only for  
9 the early stages of the signal plan; therefore, coarser time steps can be employed to “see” over  
10 a long horizon to preemptively adapt to distant platoons and other predicted long-term changes  
11 in traffic flows. To this end, we contribute the queue transmission model (QTM) which blends  
12 elements of cell-based and link-based modeling approaches to enable a non-homogeneous time  
13 MILP formulation of traffic signal control. We then experiment with this novel QTM-based MILP  
14 control in a range of traffic networks demonstrating that using non-homogeneous time steps, we  
15 can optimally solve large networks with a fraction of the MILP binary variables required to achieve  
16 the same solution quality with a homogeneous time step.

# 1 INTRODUCTION

2 As urban traffic congestion is on the increase worldwide with estimated productivity losses in the  
 3 hundreds of billions of dollars in the U.S. alone and immeasurable environmental impact (1), it is  
 4 critical to maximize capacity and throughput of existing road infrastructure through optimized traf-  
 5 fic signal control. Unfortunately, many large cities still use some degree of *fixed-time* control (2)  
 6 even if they also use *actuated* or *adaptive* control methods such as SCATS (3) or SCOOT (4).  
 7 However, there is further opportunity to improve traffic signal control even beyond adaptive meth-  
 8 ods through the use of *optimized* controllers as evidenced in a variety of approaches ranging from  
 9 mixed integer (linear) programming (5, 6, 7, 8, 9, 10) to heuristic search (11, 12) to scheduling (13)  
 10 to reinforcement learning (2). Such optimized controllers hold the promise of maximizing existing  
 11 infrastructure capacity by finding more complex (and potentially closer to optimal) jointly coor-  
 12 dinated intersection policies in comparison to heuristically-adaptive policies such as SCATS and  
 13 SCOOT. However, optimized methods are computationally demanding and often do not guarantee  
 14 *jointly* optimal solutions over a large intersection network either because (a) they only consider  
 15 coordination of neighboring intersections or arterial routes or (b) they fail to scale to large inter-  
 16 section networks simply for computational reasons. We remark that the latter scalability issue is  
 17 endemic to many mixed integer programming approaches to optimized signal control.

18 In this work, we build on the body of work in mixed integer linear programming (MILP) ap-  
 19 proaches that attempt to jointly optimize traffic signal control over an *entire traffic network* (rather  
 20 than focus on arterial routes) and specifically on improving the scalability of these methods for  
 21 large urban traffic networks. In our investigation of existing approaches in this vein, namely exem-  
 22 plar methods in the spirit of (7, 9, 10) that use a (modified) cell transmission model (CTM) (14, 15)  
 23 for their underlying prediction of traffic flows, we remark that a major drawback is the CTM-  
 24 imposed requirement to choose a predetermined *homogeneous* (and often necessarily small) time  
 25 step for reasonable modeling fidelity. This need to model a large number of CTM cells with a  
 26 small time step leads to MILPs that are exceedingly large and often intractable to solve.

27 Our primary insight in this work stems from the fact that MILP-based approaches to traffic  
 28 control used in a receding horizon control manner (that replan at fixed time intervals) need to  
 29 compute high fidelity control policies only for the early stages of the signal plan; therefore, coarser  
 30 time steps can be employed to “see” over a long horizon to preemptively adapt to distant platoons  
 31 and other predicted long-term changes in traffic flows. This need for non-homogeneous control in  
 32 turn spawns the need for an additional innovation: we require a traffic flow model that permits non-  
 33 homogeneous time steps and properly models the travel time delay between lights. To this end,  
 34 we might consider CTM extensions such as the variable cell length CTM (16), stochastic CTM  
 35 (17, 18), CTM extensions for better modeling freeway-urban interactions (19) including CTM  
 36 hybrids with link-based models (20), assymmetric CTMs for better handling flow imbalances in  
 37 merging roads (21), the situational CTM for better modeling of boundary conditions (22), and  
 38 the lagged CTM for improved modeling of the flow density relation (23). However, despite the  
 39 widespread varieties of the CTM and usage for a range of applications (24), there seems to be no  
 40 extension that permits *non-homogeneous* time steps as proposed in our novel MILP-based control  
 41 approach.

42 For this reason, as a major contribution of this work to enable our non-homogeneous  
 43 time MILP-based model of joint intersection control, we contribute the queue transmission model  
 44 (QTM) that blends elements of cell-based and link-based modeling approaches as illustrated and  
 45 summarized in Figure 1. The QTM offers the following key benefits:

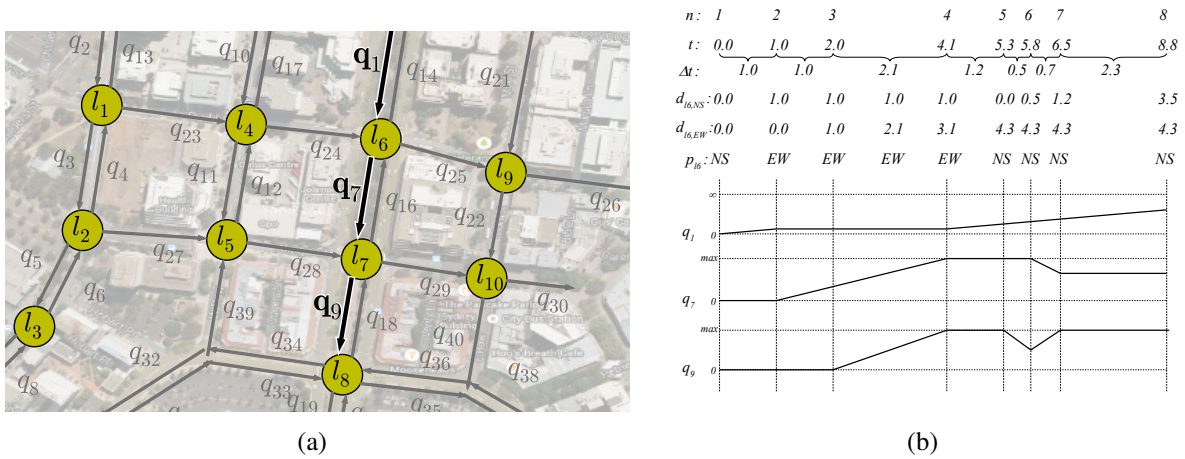


**FIGURE 1** (a) Example of a real traffic network modeled using the QTM. (b) A preview of different QTM model parameters as a function of *non-homogeneous* discretized time intervals indexed by  $n$ . For each  $n$ , we show the following parameters: the elapsed time  $t$ , the non-homogeneous time step length  $\Delta t$ , the cumulative duration  $d$  of two different light phases for  $l_6$ , the phase  $p$  of light  $l_6$ , and the traffic volume of different queues  $q$  linearly interpolated between time points. There is technically a binary  $p$  for each phase, but we abuse notation and simply show the current active phase: *NS* for *north-south green* and *EW* for *east-west green* assuming the top of the map is north. Here we see that traffic progresses from  $q_1$  to  $q_7$  to  $q_9$  according to light phases and traffic propagation delay with non-homogeneous time steps only at required changepoints. We refer to the QTM model section for precise notation and technical definitions.

- Unlike previous CTM-based joint intersection signal optimization (7, 9, 10), the QTM is intended for *non-homogeneous* time steps that can be used for control over large horizons.
- Any length of roadway with no merges or diverges can be modeled as a single queue leading to compact QTM models of large traffic networks thus maintaining relatively compact MILPs (i.e., large numbers of cells and their associated MILP variables are not required *between* intersections).
- The QTM accurately models fixed travel time delays critical to green wave coordination as in (5, 6, 8) through the use of a non-first order Markovian update model and further combines this with fully joint intersection signal optimization in the spirit of (7, 9, 10).

In the remainder of this paper, we first formalize our novel QTM model of traffic flow with non-homogeneous time steps and show how to encode it as a linear program for computing traffic flows. Next we proceed to allow the traffic signals to become discrete phase variables that are optimized subject to a delay minimizing objective and standard minimum and maximum time constraints for cycles and phases; this results in our final MILP formulation of traffic signal control. We then experiment with this novel QTM-based MILP control in a range of traffic networks demonstrating that using non-homogeneous time steps, we can optimally solve large networks with a fraction of the MILP binary variables required to achieve the same solution quality with a homogeneous time step.

## 1 THE QUEUE TRANSMISSION MODEL (QTM)

2 A Queue Transmission Model (QTM) is the tuple  $(\mathcal{Q}, \mathcal{L}, \vec{\Delta t}, \mathbf{I})$ , where  $\mathcal{Q}$  and  $\mathcal{L}$  are, respectively,  
 3 the set of queues and lights;  $\vec{\Delta t}$  is a vector of size  $N$  representing the discretization of the problem  
 4 horizon  $[0, T]$  and the duration in seconds of the  $n$ -th time interval is denoted as  $\Delta t_n$ ; and  $\mathbf{I}$  is a  
 5 matrix  $|\mathcal{Q}| \times T$  in which  $I_{i,n}$  represents the flow of cars requesting to enter queue  $i$  from the outside  
 6 of the network at time  $n$ .

7 A **traffic light**  $\ell \in \mathcal{L}$  is defined as the tuple  $(\Psi_\ell^{\min}, \Psi_\ell^{\max}, \mathcal{P}_\ell, \vec{\Phi}_\ell^{\min}, \vec{\Phi}_\ell^{\max})$ , where:

- 8 •  $\mathcal{P}_\ell$  is the set of phases of  $\ell$ ;
- 9 •  $\Psi_\ell^{\min}$  ( $\Psi_\ell^{\max}$ ) is the minimum (maximum) allowed cycle time for  $\ell$ ; and
- 10 •  $\vec{\Phi}_\ell^{\min}$  ( $\vec{\Phi}_\ell^{\max}$ ) is a vector of size  $|\mathcal{P}_\ell|$  and  $\Phi_{\ell,k}^{\min}$  ( $\Phi_{\ell,k}^{\max}$ ) is the minimum (maximum) allowed  
 11 time for phase  $k \in \mathcal{P}_\ell$ .

12 A **queue**  $i \in \mathcal{Q}$  represents a segment of road that vehicles traverse at free flow speed; once  
 13 traversed, the vehicles are vertically stacked in a stop line queue. Formally, a queue  $i$  is defined by  
 14 the tuple  $(Q_i, T_i^{\text{prop}}, F_i^{\text{out}}, \vec{F}_i, \vec{P}r_i, \mathcal{Q}_i^{\mathcal{P}})$  where:

- 15 •  $Q_i$  is the maximum capacity of  $i$ ;
- 16 •  $T_i^{\text{prop}}$  is the time required to traverse  $i$  and reach the stop line;
- 17 •  $F_i^{\text{out}}$  represents the maximum traffic flow from  $i$  to the outside of the modeled network;
- 18 •  $\vec{F}_i$  and  $\vec{P}r_i$  are vectors of size  $|\mathcal{Q}|$  and their  $j$ -th entry (i.e.,  $F_{i,j}$  and  $\text{Pr}_{i,j}$ ) represent the  
 19 maximum flow from queue  $i$  to  $j$  and the turn probability from  $i$  to  $j$  ( $\sum_{j \in \mathcal{Q}} \text{Pr}_{i,j} = 1$ ),  
 20 respectively; and
- 21 •  $\mathcal{Q}_i^{\mathcal{P}}$  denotes the set of traffic light phases controlling the outflow of queue  $i$ .

22 Differently than the CTM (9, 14), the QTM does not assume that  $\Delta t_n = T_i^{\text{prop}}$  for all  $n$ , that  
 23 is, the QTM can represent non-homogeneous time intervals (Figure 1(b)). The only requirement  
 24 over  $\Delta t_n$  is that no traffic light maximum phase time is smaller than any  $\Delta t_n$  since phase changes  
 25 occur only between time intervals; formally,  $\Delta t_n \leq \min_{\ell \in \mathcal{L}, k \in \mathcal{P}_\ell} \Phi_{\ell,k}^{\max}$  for all  $n \in \{1, \dots, N\}$ .

## 26 Computing Traffic Flows with QTM

27 In this section, we present how to compute traffic flows using QTM and non-homogeneous time  
 28 intervals  $\Delta t$ . We assume for the remainder of this section that a *valid* control plan for all traffic  
 29 lights is fixed and given as parameter; formally, for all  $\ell \in \mathcal{L}$ ,  $k \in \mathcal{P}_\ell$ , and interval  $n \in \{1, \dots, N\}$ ,  
 30 the binary variable  $p_{\ell,k,n}$  is known a priori and indicates if phase  $k$  of light  $\ell$  is active (i.e.,  $p_{\ell,k,n} =$   
 31 1) or not on interval  $n$ .

32 We represent the problem of finding the maximal flow between capacity-constrained queues  
 33 as a Linear Program (LP) over the following variables defined for all interval  $n \in \{1, \dots, N\}$  and  
 34 queues  $i$  and  $j$ :

- 35 •  $q_{i,n} \in [0, Q_i]$ : traffic volume waiting in the stop line of queue  $i$  at the beginning of  
 36 interval  $n$ ;

- $f_{i,n}^{\text{in}} \in [0, I_{i,n}]$ : inflow to the network via queue  $i$  during interval  $n$ ;
- $f_{i,n}^{\text{out}} \in [0, F_i^{\text{out}}]$ : outflow from the network via queue  $i$  during interval  $n$ ; and
- $f_{i,j,n} \in [0, F_{i,j}]$ : flow from queue  $i$  into queue  $j$  during interval  $n$ .

The maximum traffic flow from queue  $i$  to queue  $j$  is enforced by constraints (C1) and (C2). (C1) ensures that only the fraction  $\text{Pr}_{i,j}$  of the total internal outflow of  $i$  goes to  $j$ , and (C2) forces the flow from  $i$  to  $j$  to be zero if all phases controlling  $i$  are inactive (i.e.,  $p_{\ell,k,n} = 0$  for all  $k \in \mathcal{Q}_i^P$ ). If more than one phase  $p_{\ell,k,n}$  is active, then (C2) is subsumed by the domain upper bound of  $f_{i,j,n}$ .

$$f_{i,j,n} \leq \text{Pr}_{i,j} \sum_{k=1}^{|\mathcal{Q}|} f_{i,k,n} \quad (\text{C1})$$

$$f_{i,j,n} \leq F_{i,j} \sum_{p_{\ell,k,n} \in \mathcal{Q}_i^P} p_{\ell,k,n} \quad (\text{C2})$$

To simplify the presentation of remainder of the LP, we define the helper variables  $q_{i,n}^{\text{in}}$  (C3),  $q_{i,n}^{\text{out}}$  (C4), and  $t_n$  (C5) to represent the volume of traffic to enter and leave queue  $i$  during interval  $n$ , and the time elapsed since the beginning of the problem until the end of interval  $\Delta t_n$ , respectively.

$$q_{i,n}^{\text{in}} = \Delta t_n (f_{i,n}^{\text{in}} + \sum_{j=1}^{|\mathcal{Q}|} f_{j,i,n}) \quad (\text{C3})$$

$$q_{i,n}^{\text{out}} = \Delta t_n (f_{i,n}^{\text{out}} + \sum_{j=1}^{|\mathcal{Q}|} f_{i,j,n}) \quad (\text{C4})$$

$$t_n = \sum_{x=1}^n \Delta t_x \quad (\text{C5})$$

In order to account for the misalignment of the different  $\Delta t$  and  $T_i^{\text{prop}}$ , we need to find the volume of traffic that entered queue  $i$  between two arbitrary points in time  $x$  and  $y$  ( $x \in [0, T]$ ,  $y \in [0, T]$ , and  $x < y$ ), i.e.,  $x$  and  $y$  might not coincide with any  $t_n$  for  $n \in \{1, \dots, N\}$ . This volume of traffic, denoted as  $V_i(x, y)$ , is obtained by integrating  $q_{i,n}^{\text{in}}$  over  $[x, y]$  and is defined in (1) where  $m$  and  $w$  are the index of the time intervals s.t.  $t_m \leq x < t_{m+1}$  and  $t_w \leq y < t_{w+1}$ . Because the QTM dynamics are *piecewise linear*,  $q_{i,n}^{\text{in}}$  is a step function w.r.t. time and this integral reduces to the sum of  $q_{i,n}^{\text{in}}$  over the intervals contained in  $[x, y]$  and the appropriate fraction of  $q_{i,m}^{\text{in}}$  and  $q_{i,w}^{\text{in}}$  representing the misaligned beginning and end of  $[x, y]$ .

$$V_i(x, y) = (t_{m+1} - x) \frac{q_{i,m}^{\text{in}}}{\Delta t_m} + \left( \sum_{k=m+1}^{w-1} q_{i,k}^{\text{in}} \right) + (y - t_w) \frac{q_{i,w}^{\text{in}}}{\Delta t_w} \quad (1)$$

Using these helper variables, (C6) represents the flow conservation principle for queue  $i$  where  $V_i(t_{n-1} - T_i^{\text{prop}}, t_n - T_i^{\text{prop}})$  is the volume of cars that reached stop line during  $\Delta t_n$ . Since  $\vec{\Delta t}$  and  $T_i^{\text{prop}}$  for all queues are known a priori, the indexes  $m$  and  $w$  used by  $V_i$  can be pre-computed in order to encode (1); moreover, (C6) represents a non-first order Markovian update



**FIGURE 2** Cumulative arrival (blue) and departure (green) curves, and the resulting delay curve (red). The departure curve is maximized by the objective function (O1), which has the same effect as minimizing the area under the delay curve.

1 because the update considers the previous  $w - m$  time steps. To ensure that the total volume of  
 2 traffic traversing  $i$  (i.e.,  $V_i(t_n - T_i^{\text{prop}}, t_n)$ ) and waiting at the stop line does not exceed the capacity  
 3 of the queue, we apply (C7).

$$4 \quad q_{i,n} = q_{i,n-1} - q_{i,n-1}^{\text{out}} + V_i(t_{n-1} - T_i^{\text{prop}}, t_n - T_i^{\text{prop}}) \quad (\text{C6})$$

$$5 \quad V_i(t_n - T_i^{\text{prop}}, t_n) + q_{i,n} \leq Q_i \quad (\text{C7})$$

7 As with MILP formulations of CTM (e.g. Lin and Wang (9)), QTM is also susceptible to  
 8 *withholding traffic*, i.e., the optimizer might prevent cars from moving from  $i$  to  $j$  even though  
 9 the associated traffic phase is active and  $j$  is not full, e.g., this may reserve space for traffic from  
 10 an alternate approach that allows the MILP to minimize delay in the long-term even though it  
 11 leads to unintuitive traffic flow behavior. We address this well-known issue through our objective  
 12 function (O1) by maximizing the total outflow  $q_{i,n}^{\text{out}}$  (i.e., both internal and external outflow) of  $i$   
 13 plus the inflow  $f_{i,n}^{\text{in}}$  from the outside of the network to  $i$ . This quantity is weighted by the remaining  
 14 time until the end of the problem horizon  $T$  to force the optimizer to allow as much traffic volume  
 15 as possible into the network and move traffic to the outside of the network as soon as possible.

$$16 \quad \max \sum_{n=1}^N \sum_{i=1}^{|Q|} (T - t_n + 1)(q_{i,n}^{\text{out}} + f_{i,n}^{\text{in}}) \quad (\text{O1})$$

17 The objective (O1) corresponds to minimizing delay in CTM models, e.g., (O1) is equiva-  
 18 lent to the objective function (O3) in Lin and Wang (9) for their parameters  $\alpha = \beta = 1$ . Figure 2  
 19 depicts this equivalence using the cumulative number of cars entering and leaving a network as a  
 20 function of time. The delay experienced by the vehicles travelling through this network (red curve  
 21 in Figure 2) equals the horizontal difference at each point between the cumulative departure and  
 22 arrival curves (less the free flow travel time through the network). Maximizing  $q_{i,n}^{\text{out}}$  weighted by  
 23  $(T - t_n + 1)$  in (O1) is the same as forcing the departure curve to be as close as possible to the  
 24 arrival curve as early as possible; therefore, the area between arrival and departure is minimized,  
 25 which in turn minimizes the delay.



**FIGURE 3** Approximations of a queue volume obtained using homogeneous  $\Delta t = 1$ s using: (a) homogeneous  $\Delta t = 2.5$ s and 5s; and (b) non-homogeneous  $\Delta t_n \approx 0.0956n + 0.9044$  for  $n \in \{1, \dots, 17\}$ . Here we see that (b) achieves accuracy in the near-term that somewhat degrades over the long-term, where accuracy will be less critical for receding horizon control.

To illustrate the representation tradeoff offered by non-homogeneous time intervals, we computed flows and queue volumes for a fixed signal control plan derived for homogeneous  $\Delta t_n = 1$ s (ground truth) using different discretizations. Figure 3(a) shows the approximation of the ground truth using homogeneous  $\Delta t = 2.5$  and  $\Delta t = 5.0$ , and Figure 3(b) using non-homogeneous time intervals that linearly increases from 1s to 2.5s, i.e.,  $\Delta t_n \approx 0.0956n + 0.9044$  for  $n \in \{1, \dots, 17\}$ . As Figure 3(a) shows, large time steps can be rough approximations of the ground truth. Non-homogeneous discretization (Figure 3(b)) exploits this fact to provide a good approximation in the initial time steps and progressively decrease precision for points far in the future.

## 10 TRAFFIC CONTROL WITH QTM ENCODED AS A MILP

In this section, we remove the assumption that a valid control plan for all traffic lights is given and extend the LP (O1, C1–C7) to an Mixed-Integer LP (MILP) that also computes the optimal control plan. Formally, for all  $\ell \in \mathcal{L}$ ,  $k \in \mathcal{P}_\ell$ , and interval  $n \in \{1, \dots, N\}$ , the phase activation parameter  $p_{\ell,k,n} \in \{0, 1\}$  becomes a free variable to be optimized. In order to obtain a valid control



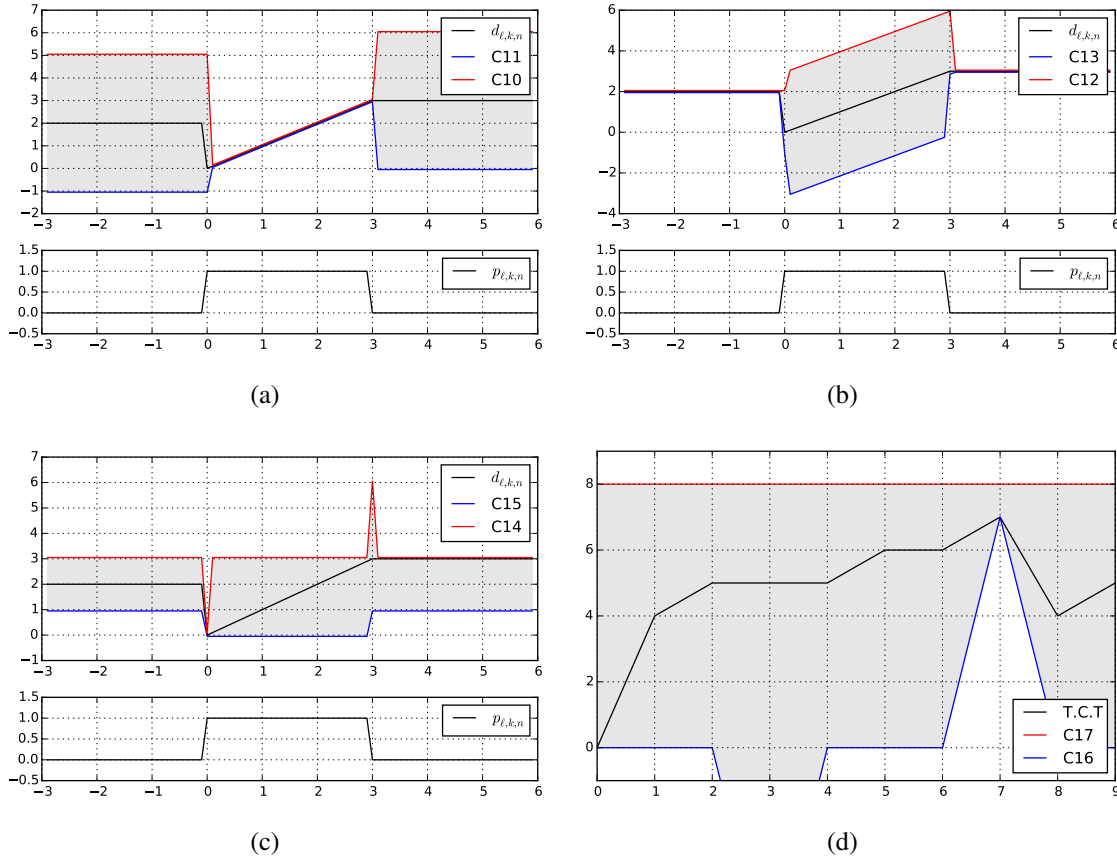


**FIGURE 4** Visualization of constraints (C10–C17) for a traffic light  $\ell$  as a function of time. (a–c) present, pairwise, the constraints (C10–C15) for phase  $k$  ( $d_{\ell,k,n}$  as the black line) and the activation variable  $p_{\ell,k,n}$  in the small plot. (d) presents the constraints for the cycle time of  $\ell$  (C16 and C17), where T.C.T. is the total cycle time and is the left hand side of both constraints. For this example,  $\Phi_{\ell,k}^{\min} = 1$ ,  $\Phi_{\ell,k}^{\max} = 3$ ,  $\Psi_{\ell}^{\min} = 7$ , and  $\Psi_{\ell}^{\max} = 8$ .

1 plan, we enforce that one phase of traffic light  $\ell$  is always active at any interval  $n$  (C8) and that  
 2 phase changes happen sequentially (C9), i.e., if phase  $k$  was active during interval  $n - 1$  and has  
 3 become inactive in interval  $n$ , then phase  $k + 1$  must be active in interval  $n$ . (C9) assumes that  
 4  $k + 1$  equals 1 if  $k = |\mathcal{P}_{\ell}|$ .

$$5 \quad \sum_{k=1}^{|\mathcal{P}_{\ell}|} p_{\ell,k,n} = 1 \quad (C8)$$

$$6 \quad p_{\ell,k,n-1} \leq p_{\ell,k,n} + p_{\ell,k+1,n} \quad (C9)$$

8 Next, we enforce the minimum and maximum phase durations (i.e.,  $\Phi_{\ell,k}^{\min}$  and  $\Phi_{\ell,k}^{\max}$ ) for  
 9 each phase  $k \in \mathcal{P}_{\ell}$  of traffic light  $\ell$ . To encode these constraints, we use the helper variable  
 10  $d_{\ell,k,n} \in [0, \Phi_{\ell,k}^{\max}]$ , defined by constraints (C10–C14), that: (i) holds the elapsed time since the  
 11 start of phase  $k$  when  $p_{\ell,k,n}$  is active (C10,C11); (ii) is constant and holds the duration of the last  
 12 phase until the next activation when  $p_{\ell,k,n}$  is inactive (C12,C13); and (iii) is restarted when phase  $k$

1 changes from inactive to active (C14). Notice that (C10–C14) employs the *big-M* method to turn  
 2 the cases that should not be active into subsumed constraints based on the value of  $p_{\ell,k,n}$ . We  
 3 use  $\Phi_{\ell,k}^{\max}$  as our large constant since  $d_{\ell,k,n} \leq \Phi_{\ell,k}^{\max}$  and  $\Delta t_n \leq \Phi_{\ell,k}^{\max}$ . Similarly, constraint (C15)  
 4 ensures the minimum phase time of  $k$  and is not enforced while  $k$  is still active. Figures 4(a)  
 5 to 4(c) present an example of how (C10–C15) work together as a function of the time  $n$  for  $d_{\ell,k,n}$ ;  
 6 the domain constraint  $0 \leq d_{\ell,k,n} \leq \Phi_{\ell,k}^{\max}$  for all  $n \in \{1, \dots, N\}$  is omitted for clarity.

$$7 \quad d_{\ell,k,n} \leq d_{\ell,k,n-1} + \Delta t_{n-1} p_{\ell,k,n-1} + \Phi_{\ell,k}^{\max}(1 - p_{\ell,k,n-1}) \quad (\text{C10})$$

$$8 \quad d_{\ell,k,n} \geq d_{\ell,k,n-1} + \Delta t_{n-1} p_{\ell,k,n-1} - \Phi_{\ell,k}^{\max}(1 - p_{\ell,k,n-1}) \quad (\text{C11})$$

$$9 \quad d_{\ell,k,n} \leq d_{\ell,k,n-1} + \Phi_{\ell,k}^{\max} p_{\ell,k,n-1} \quad (\text{C12})$$

$$10 \quad d_{\ell,k,n} \geq d_{\ell,k,n-1} - \Phi_{\ell,k}^{\max} p_{\ell,k,n-1} \quad (\text{C13})$$

$$11 \quad d_{\ell,k,n} \leq \Phi_{\ell,k}^{\max}(1 - p_{\ell,k,n} + p_{\ell,k,n-1}) \quad (\text{C14})$$

$$12 \quad d_{\ell,k,n} \geq \Phi_{\ell,k}^{\min}(1 - p_{\ell,k,n}) \quad (\text{C15})$$

14 Lastly, we constrain the sum of all the phase durations for light  $\ell$  to be within the cycle  
 15 time limits  $\Psi_{\ell}^{\min}$  (C16) and  $\Psi_{\ell}^{\max}$  (C17). In both (C16) and (C17), we use the duration of phase 1  
 16 of  $\ell$  from the previous interval  $n - 1$  instead of the current interval  $n$  because (C14) forces  $d_{\ell,1,n}$  to  
 17 be 0 at the beginning of each cycle; however, from the previous end of phase 1 until  $n - 1$ ,  $d_{\ell,1,n-1}$   
 18 holds the correct elapse time of phase 1. Additionally, (C16) is enforced right after the end of the  
 19 each cycle, i.e., when its first phase is changed from inactive to active. The value (C16) and (C17)  
 20 over time for a traffic light  $\ell$  is illustrated in Figure 4(d).

$$21 \quad d_{\ell,1,n-1} + \sum_{k=2}^{|\mathcal{P}_{\ell}|} d_{\ell,k,n} \geq \Psi_{\ell}^{\min}(p_{k,1,n} - p_{k,1,n-1}) \quad (\text{C16})$$

$$22 \quad d_{\ell,1,n-1} + \sum_{k=2}^{|\mathcal{P}_{\ell}|} d_{\ell,k,n} \leq \Psi_{\ell}^{\max} \quad (\text{C17})$$

24 The MILP that encodes the problem of finding the optimal traffic control plan in a QTM network  
 25 is defined by (O1, C1–C17).

## 26 EMPIRICAL EVALUATION

27 In this section we compare the solutions for traffic networks modeled as a QTM using homoge-  
 28 neous and non-homogeneous time intervals in two aspects: the quality of the solution and con-  
 29 vergence to the optimal solution. We compare the quality of solutions based on the total travel  
 30 time and we also consider the third quartile and maximum of the observed delay distribution. Our  
 31 hypotheses are: (i) the quality of the non-homogeneous solutions is at least as good as the homoge-  
 32 neous ones when the number of time intervals  $N$  is fixed; and (ii) the non-homogeneous approach  
 33 requires less time intervals (i.e., smaller  $N$ ) than the homogeneous approach to converge to the  
 34 optimal solution. In the remainder of this section, we present the traffic networks considered in the  
 35 experiments, our methodology, and the results.

### 36 Networks

37 We consider three networks of increasing complexity (Figure 5): an avenue crossed by three side  
 38 streets; a 2-by-3 grid; and a 3-by-3 grid with a diagonal avenue. The queues receiving cars from

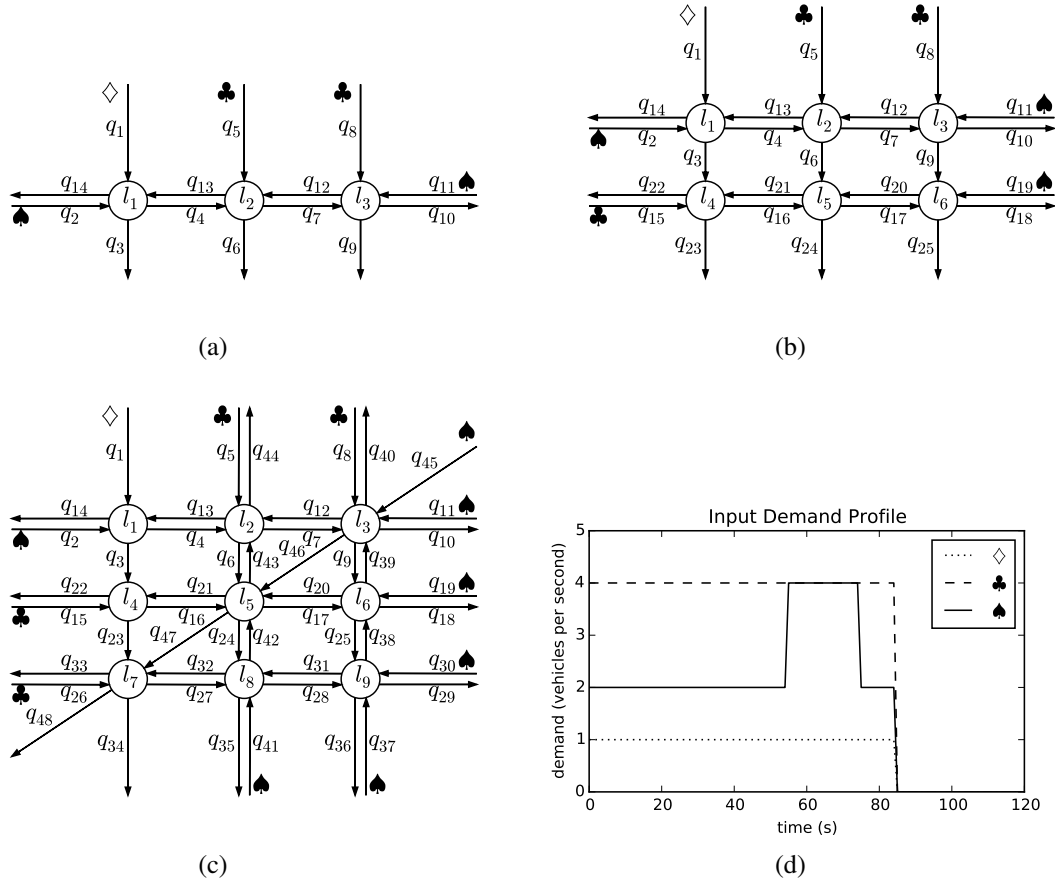


**FIGURE 5 (a–c) Networks used to evaluate the QTM performance. (d) Demand profile of the queues marked as  $\diamond$ ,  $\clubsuit$ , and  $\spadesuit$  for our experiments.**

1 outside of the network are marked in Figure 5 and we refer to them as input queues. The maxi-  
 2 mum queue capacity ( $Q_i$ ) is 60 cars for non-input queues and infinity for input queues to prevent  
 3 interruption of the input demand due to spill back from the stop line. The traversal time of each  
 4 queue  $i$  ( $T_i^{\text{prop}}$ ) is set at 9s (a distance of about 100m with a free flow speed of 50km/h). Flows are  
 5 defined from the head of each queue  $i$  into the tail of the next queue  $j$ ; there is no turning traffic  
 6 ( $\text{Pr}_{i,j} = 1$ ), and the maximum flow rate between queues,  $F_{i,j}$ , is set at 5 cars/s. All traffic lights  
 7 have two phases, north-south and east-west, and lights 2, 4 and 6 of network 3 have the additional  
 8 northeast-southwest phase to control the diagonal avenue. For networks 1 and 2,  $\Phi_{\ell,k}^{\min}$  is 1s,  $\Phi_{\ell,k}^{\max}$   
 9 is 3s,  $\Psi_{\ell}^{\min}$  is 2s, and  $\Psi_{\ell}^{\max}$  is 6s, for all traffic light  $\ell$  and phase  $k$ . For network 3,  $\Phi_{\ell,k}^{\min}$  is 1s and  
 10  $\Phi_{\ell,k}^{\max}$  is 6s for all  $\ell$  and  $k$ ; and  $\Psi_{\ell}^{\min}$  is 2s and  $\Psi_{\ell}^{\max}$  is 12s for all lights  $\ell$  except for lights 2, 4 and  
 11 6 (i.e., lights also used by the diagonal avenue) in which  $\Psi_{\ell}^{\min}$  is 3s and  $\Psi_{\ell}^{\max}$  is 18s.

## 12 Experimental Methodology

13 For each network, a constant background level traffic is injected in the network in the first 55s to  
 14 allow the solver to settle on a stable policy. Then a spike in demand is introduced in the queues  
 15 marked as  $\spadesuit$  (Figure 5) from time 55s to 70s to trigger a policy change. From time 70s to 85s,  
 16 the demand is returned to the background level, and then reduced to zero for all input queues. We



**FIGURE 6 Receding horizon control.** In this example, the problem horizon  $T$  is 40s. The major frames are discretized in 12 time intervals ( $N = 12$ ) and they span 15s and 30s for homogeneous and non-homogeneous discretizations, respectively.

1 extend the problem horizon  $T$  until all cars have left the network. By clearing the network, we can  
 2 easily measure the total travel time for all the traffic as the area between the cumulative arrival and  
 3 departure curves measured at the boundaries of the network. The background level for the input  
 4 queues are 1, 4 and 2 cars/s for queues marked as  $\diamond$ ,  $\clubsuit$  and  $\spadesuit$  (Figure 5(d)), respectively; and  
 5 during the high demand period, the queues  $\spadesuit$  receive 4 cars/s.

6 For both homogeneous and non-homogeneous intervals, we use the MILP QTM formula-  
 7 tion in a receding horizon manner: a control plan is computed for a pre-defined horizon (smaller  
 8 than  $T$ ) and only a prefix of this plan is executed before generating a new control plan. Figure 6  
 9 depicts our receding horizon approach and we refer to the planning horizon as a major frame and  
 10 its executable prefix as a minor frame. Notice that, while the plan for a minor frame is being  
 11 executed, we can start computing the solution for the next major frame based on a forecast model.

12 To perform a fair comparison between the homogeneous and non-homogeneous discretiza-  
 13 tions, we fix the size of all minor frames to 10s and force it to be discretized in homogeneous  
 14 intervals of 0.25s. For the homogeneous experiments,  $\Delta t$  is kept at 0.25s throughout the major  
 15 frame; therefore, given  $N$ , the major frame size equals  $N/4$  seconds for the homogeneous ap-  
 16 proach. For the non-homogeneous experiments,  $\Delta t$  linearly increases from 0.25s at the end of  
 17 the minor frame to 1.0s at the end of the major frame; therefore, the major frame size used by  
 18 the non-homogeneous approach is  $10.375 + 0.625(N - 40)$  seconds for a given  $N > 40$ . Once  
 19 we have generated a series of minor frames, we concatenate them into a single plan and compute  
 20 the flow through the network using the QTM LP formulation with a fixed (homogeneous)  $\Delta t$  of  
 21 0.25s. We also compare both receding horizon approaches against the optimal solution obtained  
 22 by computing a single control plan for the entire control horizon (i.e.,  $[0, T]$ ) using a fixed  $\Delta t$  of  
 23 0.25s.

24 For all our experiments, we used Gurobi<sup>TM</sup> as MILP solver with 12 threads on a 3.1GHz  
 25 AMD Opteron<sup>TM</sup> 4334 processor with 12 cores. We limit the MIP gap accuracy to 0.1% and the  
 26 time cutoff for solving a major frame to 3000s for the receding horizon approaches and unbounded  
 27 for the optimal plan. All our results are averaged over five runs to account for Gurobi's stochastic  
 28 strategies.

## 29 Results

30 Figures 7(a), 7(c) and 7(e) show, for each network, the increase in the total travel time w.r.t. the  
 31 optimal solution as a function of  $N$ . As we hypothesized, the non-homogeneous discretization re-

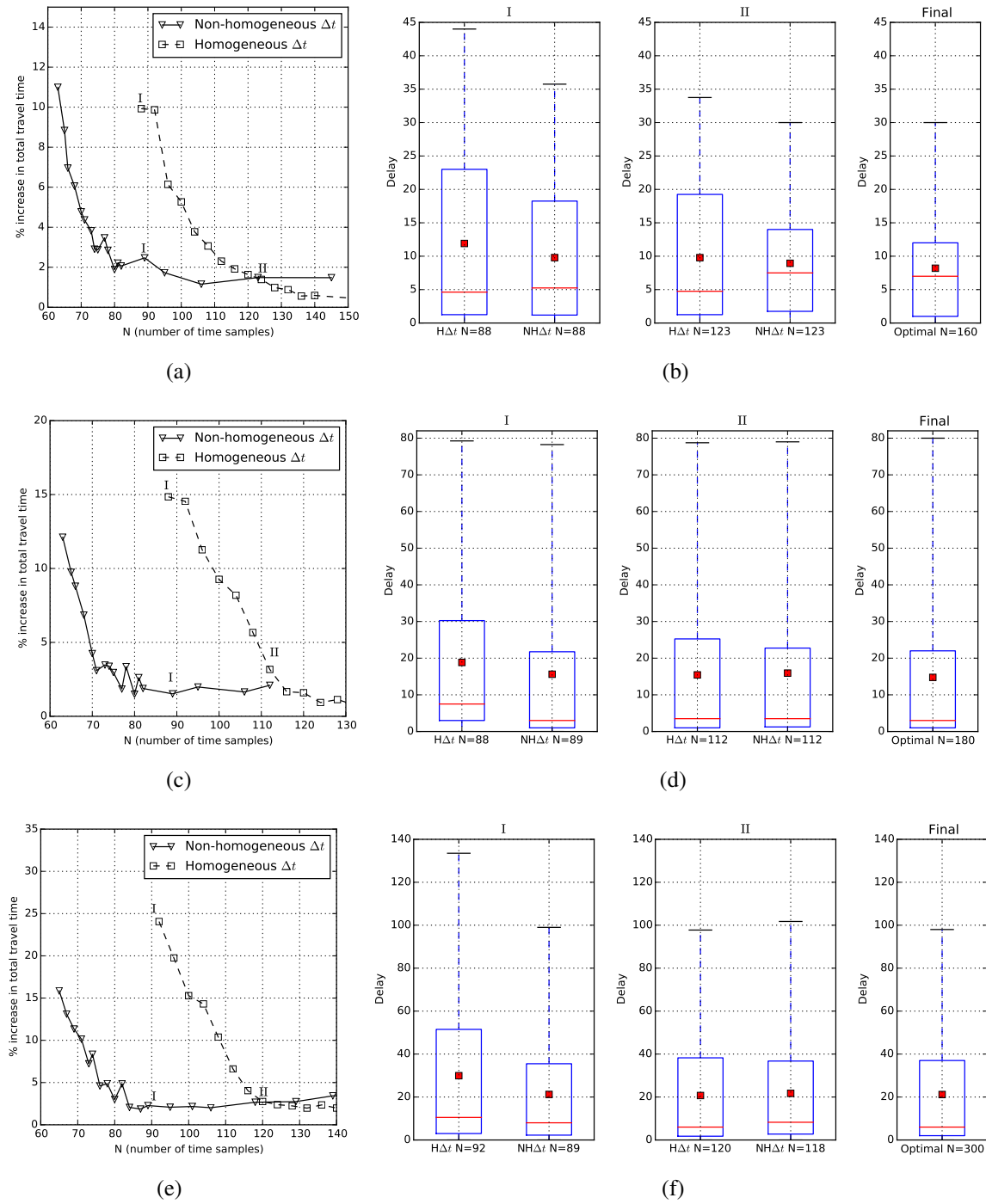


**FIGURE 7** Increase in the total travel time w.r.t. the optimal solution as a function of  $N$  (Figures a, c, and e) and distribution of the total delay of each car for different values of  $N$  (Figures b, d, and f). For each row, the roman numeral on top of the box plots corresponds to point the travel time plot marked with the same numeral. The mean of the total delay is presented as a red square in box plots. Plots in the  $i$ -th row correspond to the results for the  $i$ -th network in Figure 5.

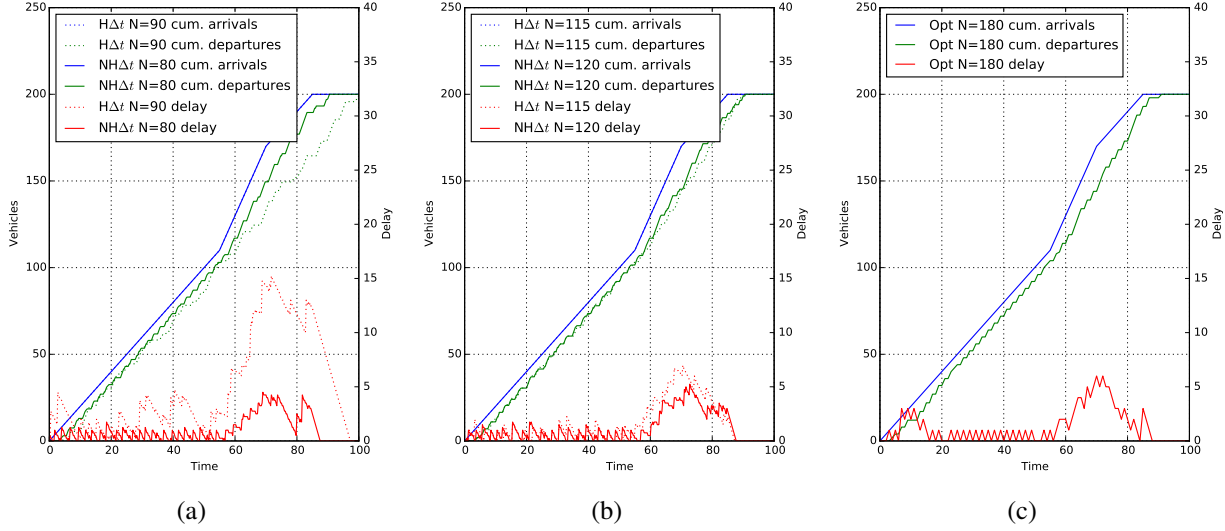


**FIGURE 8** Cumulative arrival and departure curves and delay for queue 1 in the 2-by-3 network (Figure 5(b)). The value of  $N$  in plots (a) and (b) corresponds, respectively, to the convergence point of the non-homogeneous and homogeneous approaches (Figure 7(c)). (c) presents the same curves for the optimal solution.

quires less time intervals (i.e., smaller  $N$ ) to obtain a solution with the same total travel time. This is important because the size of the MILP, including the number of binary variables, scales linearly with  $N$ ; therefore, the non-homogeneous approach can scale up better than the homogeneous one (e.g., Figure 7(e)). Also, for homogeneous and non-homogeneous discretizations, finding the optimal solution of major frames with large  $N$  might require more time than our imposed 3000s time cutoff and, in this case, Gurobi returns a feasible control plan that is far from optimal. The effect in the total travel time of these poor solutions can be seen in Figure 7(e) for  $N > 120$ .

The distribution of the total delay observed by each car while traversing the network is shown in Figures 7(b), 7(d) and 7(f). Each group of box plots represents a different value of  $N$ : when the non-homogeneous  $\Delta t$  first converges; when the homogeneous  $\Delta t$  first converges; and the optimum solution itself. In all networks, the quality of the solution obtained using non-homogeneous  $\Delta t$  is better or equal than using homogeneous  $\Delta t$  for fixed  $N$  in both the total travel time and *fairness*, i.e., smaller third quartile and maximum delay.

To further illustrate the differences between homogeneous and non-homogeneous discretizations, Figure 8 shows the cumulative arrival and departure curves and the how delay evolves over time for  $q_1$  of network 2 (Figure 5(b)). In Figure 8(a), the comparison is done when non-homogeneous  $\Delta t$  first converges (i.e., point I in Figure 7(c)) and for this value of  $N$ , the major frame size in seconds of the non-homogeneous approach is 19.125s longer than the homogeneous one. This allows the MILP solver to “see” 19s further in the future when using non-homogeneous discretization and find a coordinated signal policy along the avenue to dissipate the extra traffic that arrives at time 55s. The shorter major frame of the homogeneous discretization does not allow the solver to adapt this far in advance and its delay observed after 55s is much larger than the non-homogeneous one. Once the homogeneous  $\Delta t$  has converged (Figure 8(b)), it is also able to anticipate the increased demand and adapt well in advance and both approaches generate solutions

1 close to optimum (Figure 8(c)).

## 2 CONCLUSION

3 In this paper, we showed how to formulate a novel queue transmission model (QTM) model of  
 4 traffic flow with non-homogeneous time steps as a linear program. We then proceeded to allow the  
 5 traffic signals to become discrete variables subject to a delay minimizing optimization objective  
 6 and standard traffic signal constraints leading to a final MILP formulation of traffic signal control.  
 7 We experimented with this novel QTM-based MILP control in a range of networks and demon-  
 8 strated that by exploiting the non-homogeneous time steps supported by the QTM, we are able  
 9 to scale the model up to larger networks whilst maintaining the same quality of a homogeneous  
 10 solution using more binary variables. Altogether, this work represents a major step forward in the  
 11 scalability of MILP-based jointly optimized traffic signal control via the use of a non-homogeneous  
 12 traffic models and thus helps pave the way for fully optimized joint urban traffic signal controllers  
 13 as an improved successor technology to existing signal control methods.

## 14 ACKNOWLEDGMENT

15 This work is part of the Advanced Data Analytics in Transport programme, and supported by Na-  
 16 tional ICT Australia (NICTA) and NSW Trade&Investment. NICTA is funded by the Australian  
 17 Government through the Department of Communications and the Australian Research Council  
 18 through the ICT Centre of Excellence Program. NICTA's role is to pursue potentially economi-  
 19 cally significant ICT related research for the Australian economy. NSW Trade&Investment is the  
 20 business development agency for the State of New South Wales.

## 21 REFERENCES

- 22 [1] Bazzan, A. L. C. and F. Klügl, *Introduction to Intelligent Systems in Traffic and Transporta-*  
 23 *tion*. Synthesis Lectures on Artificial Intelligence and Machine Learning, Morgan & Claypool  
 24 Publishers, 2013.
- 25 [2] El-Tantawy, S., B. Abdulhai, and H. Abdelgawad, Multiagent reinforcement learning for  
 26 integrated network of adaptive traffic signal controllers (MARLIN-ATSC): methodology  
 27 and large-scale application on downtown toronto. *Intelligent Transportation Systems, IEEE*  
 28 *Transactions on*, Vol. 14, No. 3, 2013, pp. 1140–1150.
- 29 [3] Sims, A. G. and K. W. Dobinson, SCAT–The Sydney co-ordinated adaptive traffic system:  
 30 Philosophy and benefits. *IEEE Transactions on Vehicular Technology*, Vol. 29, 1980.
- 31 [4] Hunt, P. B., D. I. Robertson, R. D. Bretherton, and R. I. Winton, *SCOOT–A traffic responsive*  
 32 *method of coordinating signals*. Transportation Road Research Lab, Crowthorne, U.K., 1981.
- 33 [5] Gartner, N., J. D. Little, and H. Gabbay, *Optimization of traffic signal settings in networks by*  
 34 *mixed-integer linear programming*. DTIC Document, 1974.
- 35 [6] Gartner, N. H. and C. Stamatiadis, Arterial-based control of traffic flow in urban grid net-  
 36 works. *Mathematical and computer modelling*, Vol. 35, No. 5, 2002, pp. 657–671.
- 37 [7] Lo, H. K., A novel traffic signal control formulation. *Transportation Research Part A: Policy*  
 38 *and Practice*, Vol. 33, No. 6, 1998, pp. 433–448.

- 1 [8] He, Q., K. L. Head, and J. Ding, PAMSCOD: Platoon-based Arterial Multi-modal Signal  
2 Control with Online Data. *Procedia-Social and Behavioral Sciences*, Vol. 17, 2011, pp. 462–  
3 489.
- 4 [9] Lin, W.-H. and C. Wang, An enhanced 0-1 mixed-integer LP formulation for traffic signal  
5 control. *Intelligent Transportation Systems, IEEE Transactions on*, Vol. 5, No. 4, 2004, pp.  
6 238–245.
- 7 [10] Han, K., T. L. Friesz, and T. Yao, A link-based mixed integer LP approach for adaptive traffic  
8 signal control. *arXiv preprint arXiv:1211.4625*, 2012.
- 9 [11] Lo, H. K., E. Chang, and Y. C. Chan, Dynamic network traffic control. *Transportation Re-*  
10 *search Part A: Policy and Practice*, Vol. 35, No. 8, 1999, pp. 721–744.
- 11 [12] He, Q., W.-H. Lin, H. Liu, and K. L. Head, Heuristic algorithms to solve 0–1 mixed integer  
12 LP formulations for traffic signal control problems. In *Service Operations and Logistics and*  
13 *Informatics (SOLI), 2010 IEEE International Conference on*, IEEE, 2010, pp. 118–124.
- 14 [13] Smith, S., G. Barlow, X.-F. Xie, and Z. Rubinstein, SURTRAC: Scalable Urban Traffic Con-  
15 trol. In *Transportation Research Board 92nd Annual Meeting Compendium of Papers*, Trans-  
16 portation Research Board, 2013.
- 17 [14] Daganzo, C. F., The cell transmission model: A dynamic representation of highway traffic  
18 consistent with the hydrodynamic theory. *Transportation Research Part B: Methodological*,  
19 Vol. 28, No. 4, 1994, pp. 269–287.
- 20 [15] Daganzo, C. F., The cell transmission model, part II: network traffic. *Transportation Research*  
21 *Part B: Methodological*, Vol. 29, No. 2, 1995, pp. 79–93.
- 22 [16] Xiaojian, H., W. Wei, and H. Sheng, Urban traffic flow prediction with variable cell trans-  
23 mission model. *Journal of Transportation Systems Engineering and Information Technology*,  
24 Vol. 10, No. 4, 2010, pp. 73–78.
- 25 [17] Sumalee, A., R. Zhong, T. Pan, and W. Szeto, Stochastic cell transmission model (SCTM): A  
26 stochastic dynamic traffic model for traffic state surveillance and assignment. *Transportation*  
27 *Research Part B: Methodological*, Vol. 45, No. 3, 2011, pp. 507–533.
- 28 [18] Jabari, S. E. and H. X. Liu, A stochastic model of traffic flow: Theoretical foundations.  
29 *Transportation Research Part B: Methodological*, Vol. 46, No. 1, 2012, pp. 156–174.
- 30 [19] Huang, K. C., *Traffic Simulation Model for Urban Networks: CTM-URBAN*. Ph.D. thesis,  
31 Concordia University, 2011.
- 32 [20] Muralidharan, A., G. Dervisoglu, and R. Horowitz, Freeway traffic flow simulation using the  
33 link node cell transmission model. In *American Control Conference, 2009. ACC'09.*, IEEE,  
34 2009, pp. 2916–2921.
- 35 [21] Gomes, G. and R. Horowitz, Optimal freeway ramp metering using the asymmetric cell trans-  
36 mission model. *Transportation Research Part C: Emerging Technologies*, Vol. 14, No. 4,  
37 2006, pp. 244–262.



- 1 [22] Kim, Y., *Online traffic flow model applying dynamic flow-density relation*. Int. At. Energy  
2 Agency, 2002.
- 3 [23] Lu, S., S. Dai, and X. Liu, A discrete traffic kinetic model—integrating the lagged cell trans-  
4 mission and continuous traffic kinetic models. *Transportation Research Part C: Emerging*  
5 *Technologies*, Vol. 19, No. 2, 2011, pp. 196–205.
- 6 [24] Alecsandru, C., A. Quddus, K. C. Huang, B. Rouhieh, A. R. Khan, and Q. Zeng, An as-  
7 sessment of the cell-transmission traffic flow paradigm: Development and applications. In  
8 *Transportation Research Board 90th Annual Meeting*, 2011, 11-1152.